JOURNAL OF GEOPHYSICAL RESEARCH, VOL. 96, NO. B2, PAGES 2057–2069, FEBRUARY 10, 1991

Diffusion Domains Determined by ^{39}Ar Released During Step Heating

OSCAR M. LOVERA[1] AND FRANK M. RICHTER

Department of the Geophysical Sciences, University of Chicago, Illinois

T. MARK HARRISON

Department of Earth and Space Sciences, University of California, Los Angeles

The Arrhenius plot for ^{39}Ar released during step heating of a sample containing a distribution of diffusion domains will depart from a straight line in ways that depend on the domain size distribution and the heating schedule used to extract the ^{39}Ar. In a new series of experiments we make use of the heating schedule effect to confirm the multidomain nature of several alkali feldspar samples. We find that temperature cycling is particularly useful for determining the diffusion parameters (activation energy and frequency factor) of the different domains. We also use the log (r/r_0) versus cumulative percent ^{39}Ar released plot presented in an earlier paper to display better the sizes of the different domains and the proportion of argon that they contain. We conclude by showing that a particular choice of the geometry and number of domains is not critical to the determination of the thermal history provided the ^{39}Ar data are satisfactorily fitted by the particular choice mode. Experiments on single crystals show that multiple diffusion domains are an intrinsic property of the feldspars and thus are not separable by a careful selection of the grains to be analyzed.

INTRODUCTION

Recent work on argon diffusion [*Zeitler*, 1987; *Lovera et al.*, 1989; *Richter et al.*, 1991], as well as inferences from microstructural studies [*Harrison and McDougall*, 1981], suggest that feldspars contain argon diffusion domains of varying sizes. Earlier studies by *Turner* [1968] and *Gillespie et al.* [1982] illustrated the effect on the age spectra of aggregate samples having a distribution of different argon domains. Our own results [*Lovera et al.*, 1989] not only support the general concept of distinct diffusion domains in alkali feldspars but also quantify the differences that should be expected between age spectra, Arrhenius plots, and cooling histories calculated assuming single or multi-diffusion-domain behavior. When data from alkali feldspar samples of the Chain of Ponds pluton (CPP) are interpreted as having a single uniform domain, we found that the cooling history determined from their closure temperatures (calculated following *Dodson* [1973]) disagrees with estimates of the cooling rate obtained from the shape of the individual age spectra. These differences are reconciled once one assumes that the samples from CPP are in fact made up of a distribution of different diffusion domain sizes. The most direct consequence of the existence of different size diffusion domain is the observed departure from linearity of diffusion coefficient calculated from ^{39}Ar versus reciprocal temperature in the Arrhenius plot.

In our previous work we assumed that all diffusion domains in the sample share the same activation energy, but the data presented did not clearly resolve the activation energy of each component of the distribution. Data presented here will further demonstrate the existence of a distribution of diffusion domain sizes in feldspar samples and also will show how the heating schedule can be optimized for determining the activation energy of each component of the domain size distribution. We noted earlier that Arrhenius plots derived from multidomain samples depend on the temperature and duration of the heating steps used. In other words, different heating schedules for the same sample will result in different Arrhenius plots. We present the results of applying different heating schedules (cycling the temperature rather than monotonically increasing it) to splits of samples from CPP. Comparing these results with those obtained previously using progressively increasing temperature steps [*Heizler et al.*, 1988] further shows that the alkali feldspars from CPP contain diffusion domains of varying sizes.

The new cyclic heating experiments generally confirm as a valid approximation to assume that all domains have the same activation energy. In another paper [*Harrison et al.*, 1991] we recognize the existence of small variations in activation energies and describe an approach that accommodated these variations in the multidomain calculations. However, the Arrhenius plots from these examples fail to show the properties of the distribution itself (domain size, ρ_j, and volume fraction, ϕ_j). We proposed [*Richter et al.*, 1991] a new way of plotting the data, which, being independent of E, D_0, and the heating schedule, better displays the distribution properties. We present a simple method to calculate the distribution parameters involved (ρ_j, ϕ_j) using this new graph. Also, we analyze the role of the distribution parameters in determining the estimate of the cooling history. The final section contains new data from single crystal samples. Since these samples also contain a distribution of diffusion domain sizes, it appears that careful sample selection does not obviate the need for an interpretative scheme based on a distribution of domain sizes.

ANALYTICAL METHODS

The $^{40}Ar/^{39}Ar$ isotopic measurements of alkali-feldspar separates were obtained using automated Nuclide 4.5-60-

[1]Now at Division of Geological and Planetary Sciences, California Institute of Technology, Pasadena.

Paper number 90JB02217.
0148-0227/91/90JB-02217$05.00

RSS and VG 1200S mass spectrometers at the State University of New York at Albany following the analytical procedures of *Harrison and Fitz Gerald* [1986]. Samples weighing from 0.2 to ~100 mg were wrapped in Sn foil and irradiated in evacuated quartz vials along with Fe-mica biotite (307.3 Ma) flux monitors, K_2SO_4 and CaF_2 in the H-5 position of the Ford Reactor, University of Michigan. Samples were heated in a Ta crucible within a double-vacuum furnace modified in the fashion described by *Harrison and Fitz Gerald* [1986] from the design of *Staudacher et al.* [1978]. Precision of temperature measurement and control is estimated to be better than ±1°C for most conditions and accuracy of measurement of thermocouple temperature is ±5°C. The accuracy of measurement of the sample temperature can be routinely gauge by the melting temperature of the Sn foil (at 230°C) and the breakdown of volume diffusion behavior in the alkali feldspar at 1150°C due to incongruent melting. Because each heating step involves a heat-up and cool-down phase, the duration of each step is taken to be the time between reaching within about 5°C of designated temperature and the furnace shutdown. Although the time for thermal equilibration within the sample crucible varies with temperature, the effect on calculated diffusion coefficients is second order and no correction is made for steps greater than two minutes. Note that the heating schedule which optimizes the information on the Arrhenius plot may not yield the best age spectrum. Indeed, there is a clear conflict between these goals which requires compromises in the choice of the heating schedule. For example, as discussed in the next section, steps cycled to lower temperature to assess variation in activation energy between domains result in very low gas yield, even for long heating durations. While the ^{39}Ar signal is almost always sufficient for the Arrhenius calculations, the corresponding radiogenic ^{40}Ar content is often highly uncertain giving the age spectrum a noisy appearance (e.g., Figure 5). Details of the calculations and the FORTRAN 77 programs used to fit the empirical results to theory are given by O. M. Lovera (^{40}Ar/^{39}Ar diffusion from multi-domain samples, submitted to *Computers and Geosciences*, 1990).

Extraction blanks have varied over the course of these analyses from 7×10^{-16} to 10^{-14} mol ^{40}Ar in an atmospheric ratio, with the VG1200S system attaining the very lowest values. There is effectively no ^{39}Ar blank in either system even for long-term heating steps of up to 3 days. Gettering of reactive gases is accomplished by the hot Ta furnace walls and SAES Zr-Ti alloy pumps (Nuclide, one 50 L/s (400°C) and one 10 L/s (100°C); VG, one 10 L/s (700°C)]. The ^{40}Ar/^{39}Ar analytical results and heating schedules are given in Tables 1–4. Corrections are made to the data for interfering nuclear reaction products, extraction blanks, and the decay of ^{37}Ar. Uncertainties for ages are quoted at the one sigma level and do not include the error in the J factor, estimated to be 0.5%. All ages have been calculated with the decay constants and isotope abundances recommended by *Steiger and Jäger* [1977]. Diffusion coefficients are calculated using the expressions summarized in Table 5.1 of *McDougall and Harrison* [1988] and are given, together with the log (D/r^2) and log (r/r_0) data in Tables 1–4. We note here that the nature of our samples and the step heating approach precludes assessment of uncertainty of the cumulative percent ^{39}Ar released because each step is dependent on all the previous steps. Also, exact duplication of the data is somewhat unreachable since each grain may have a different domain distribution.

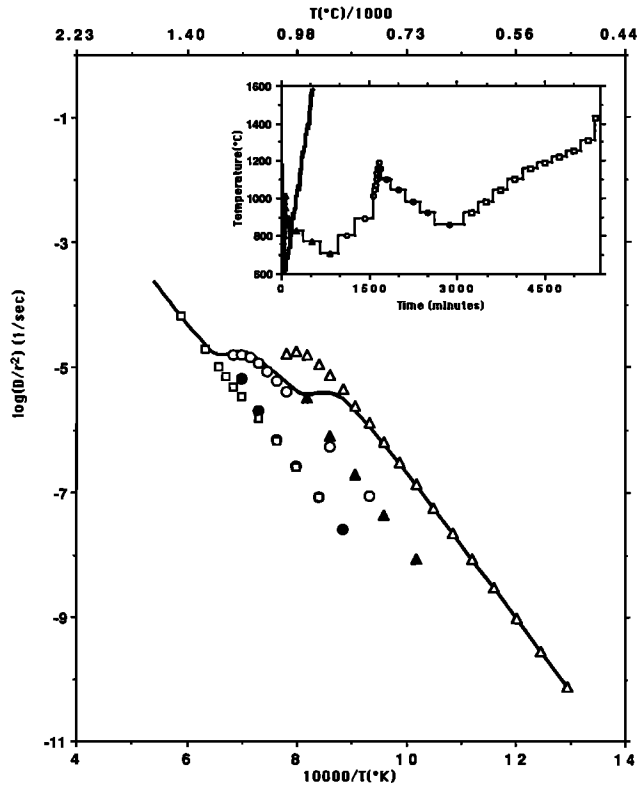

Fig. 1. Computed Arrhenius plots obtained by applying two different heating schedules to the same theoretical sample (one increasing the temperature monotonically, and the other cycling the temperature). The cycled heating schedule shown in the inset (line with symbols) starts by increasing the temperature much like the monotonic heating (heavy line), but now using shorter time steps and avoiding incipient melting (open triangles). The temperature then is reduced (solid triangles), and later cycled (first open circles, later solid circles, and finally open squares). The Arrhenius plots (using the same symbols and a heavy line in the monotonic case) show that at first one obtains information on the properties of the smallest domains but that as the extraction of argon continues, the contributions from the larger domains begin to be mapped out. This figure shows that the cycled heating schedule provides a better measure of the activation energy of the different domains.

CYCLING THE EXTRACTION TEMPERATURES

Based on data generated by monotonically increasing extraction temperatures, we made the simple assumption that all domains have the same activation energy [*Lovera et al.*, 1989]. However, we noted that Arrhenius plots obtained using the traditional monotonic step heating do not resolve well the activation energy of the larger domain sizes. In order to determine the activation energy of each component of the distribution, we find it to be more effective to cycle the temperature rather than to increase it monotonically. As an example, Figure 1 shows calculated Arrhenius data for both a monotonic and cyclic heating experiment applied to the same synthetic sample. The cyclic heating schedule begins by raising the temperature in the conventional way, but using shorter time steps than those used in the monotonic experiment. Shorter time steps shift the departure from linear behavior in the Arrhenius plot to higher temperatures.

TABLE 1. MH-10.cf K-Feldspar

Temperature, °C	$^{40}Ar/^{39}Ar$	$^{37}Ar/^{39}Ar$	$^{36}Ar/^{39}Ar$ (E-3)	$^{39}Ar_K$ (E-13 mol)	Percent $^{39}Ar_K$ Released	^{40}Ar, %	$^{40}Ar^*/^{39}Ar_K$	Age ± 1 s.d., Ma	Time, min	10000/T, °K	log (D/r^2), s^{-1}	log (r/r_0)
450	342.70	0.068	467.30	0.19	0.10	59.4	204.50	1279.0 ± 14.3	71	13.83	−10.69	−0.036
520	149.90	0.087	90.01	0.36	0.29	81.8	123.30	872.5 ± 20.8	43	12.61	−9.60	0.044
580	72.33	0.034	25.83	1.03	0.83	89.0	64.67	509.3 ± 3.1	40	11.72	−8.65	0.023
650	43.17	0.032	12.73	2.81	2.32	9.10	39.37	326.8 ± 1.4	31	10.83	−7.65	−0.021
400	4455.00	0.471	15524.00	0.03	2.33	0.0	0.00	0.0 ± 0.0	990	14.86	−11.16	−0.328
720	35.22	0.041	3.26	3.33	4.09	96.9	34.22	287.3 ± 1.6	13	10.07	−6.89	−0.011
800	35.34	0.040	1.93	7.51	8.06	98.2	34.73	291.2 ± 0.9	10	9.32	−6.13	−0.008
870	35.34	0.033	1.56	6.32	11.40	98.5	34.85	292.1 ± 0.6	4	8.75	−5.59	0.014
1000	38.03	0.025	0.33	16.80	20.20	99.6	37.89	315.5 ± 0.3	3	7.86	−4.81	0.079
1000	40.64	0.013	0.97	8.22	24.60	99.1	40.31	333.9 ± 0.5	5	7.86	−5.16	0.255
1000	41.81	0.012	1.63	6.79	28.20	98.7	41.29	341.3 ± 0.4	10	7.86	−5.46	0.404
1000	42.54	0.011	2.27	4.88	30.70	98.2	41.84	345.4 ± 1.5	10	7.86	−5.54	0.445
1000	43.03	0.010	3.21	4.55	33.10	97.6	42.04	346.9 ± 1.3	14	7.86	−5.67	0.510
1000	43.24	0.003	4.36	2.06	34.20	96.6	41.92	346.0 ± 3.0	7	7.86	−5.68	0.515
750	217.50	0.241	585.70	0.11	34.30	20.2	44.38	364.5 ± 62.5	112	9.78	−8.13	0.757
650	2336.00	0.014	8071.00	0.06	34.40	0.0	0.00	0.0 ± 0.0	1037	10.83	−9.40	0.854
850	63.18	0.003	62.16	0.30	34.50	69.8	44.78	367.4 ± 8.3	46	8.90	−7.31	0.797
950	44.94	0.012	8.80	1.25	35.10	93.6	42.30	348.9 ± 2.4	17	8.18	−6.26	0.641
1000	43.43	0.002	3.36	2.73	36.60	97.4	42.40	349.6 ± 2.1	16	7.86	−5.88	0.615
1000	43.72	0.013	6.79	2.85	38.10	95.1	41.68	344.2 ± 1.6	20	7.86	−5.93	0.640
1050	42.91	0.019	5.06	2.35	39.30	96.2	41.38	342.0 ± 1.0	7	7.56	−5.53	0.594
1100	42.84	0.020	1.48	4.42	41.70	98.7	42.37	349.4 ± 1.3	7	7.28	−5.23	0.587
1150	43.32	0.030	1.73	6.99	45.40	98.6	42.78	352.5 ± 0.9	7	7.03	−4.98	0.589
1150	43.63	0.025	2.03	6.35	48.70	98.4	43.00	354.1 ± 1.2	11	7.03	−5.16	0.679
1150	43.89	0.022	1.90	5.81	51.80	98.5	43.29	356.3 ± 0.9	15	7.03	−5.29	0.745
1150	44.46	0.023	1.91	5.24	54.5	98.5	43.86	360.5 ± 1.6	20	7.03	−5.41	0.804
1150	44.97	0.024	3.96	5.94	57.7	97.2	43.77	359.9 ± 1.1	31	7.03	−5.50	0.849
1150	45.59	0.022	5.18	7.34	61.6	96.5	44.03	361.8 ± 0.5	60	7.03	−5.64	0.920
1150	46.02	0.017	6.13	11.10	67.4	95.9	44.17	362.9 ± 0.5	146	7.03	−5.77	0.984
950	93.54	0.031	177.50	1.63	68.3	43.8	41.04	339.4 ± 4.2	852	8.18	−7.32	1.171
1200	45.32	0.017	2.43	3.65	70.2	98.2	44.57	365.8 ± 1.5	8	6.79	−4.91	0.677
1200	44.55	0.006	0.84	8.13	74.5	99.3	44.27	363.6 ± 0.4	15	6.79	−4.78	0.612
1200	44.52	0.009	1.50	8.94	79.2	98.8	44.04	361.9 ± 0.6	20	6.79	−4.78	0.612
1200	44.56	0.003	0.40	6.83	82.8	99.6	44.41	364.6 ± 0.7	20	6.79	−4.80	0.622
1200	44.75	0.007	1.03	5.24	85.6	99.1	44.41	364.7 ± 0.6	20	6.79	−4.83	0.637
1200	44.64	0.017	3.95	5.97	88.7	97.2	43.44	357.4 ± 0.1	30	6.79	−4.86	0.652
1300	46.13	0.087	5.95	12.50	95.3	96.0	44.33	364.0 ± 28.1	5	6.36	−3.53	0.207
1330	44.70	0.008	1.19	4.22	97.6	99.0	44.31	363.9 ± 0.6	5	6.24	−3.66	0.344
1360	44.99	0.005	5.63	1.25	98.2	95.7	43.29	356.3 ± 2.5	5	6.12	−3.97	0.551
1390	45.16	0.018	6.62	0.95	98.7	94.9	43.17	355.4 ± 4.1	10	6.01	−4.25	0.747
1450	45.28	0.034	9.78	0.65	99.1	92.6	42.36	349.3 ± 4.7	10	5.80	−4.27	0.865
1550	45.15	0.012	3.80	1.76	100.0	97.1	43.99	361.6 ± 1.9				

J = 0.005044, weight = 0.11400 g, E = 49.22 kcal/mol, log (D_0/r_0^2) = 4.049 s^{-1}, spherical model.

TABLE 2. MH-10.bm K-Feldpsar

Temperature, °C	$^{40}Ar/^{39}Ar$	$^{37}Ar/^{39}Ar$	$^{36}Ar/^{39}Ar$ (E-3)	$^{39}Ar_K$ (E-13 mol)	Percent $^{39}Ar_K$ Released	$^{40}Ar^*$, %	$^{40}Ar^*/^{39}Ar_K$	Age ± 1 s.d., Ma	Time, min	10000/T, °K	Log (D/r^2), s^{-1}	log (r/r_0)
500	277.20	0.284	158.20	0.27	0.2	83.0	230.50	1391.0 ± 6.6	23	12.94	−9.596	−0.083
600	61.83	0.129	8.26	1.11	1.0	95.9	59.36	472.5 ± 2.4	17	11.45	−8.074	−0.043
700	36.62	0.149	2.28	3.63	3.7	98.0	35.93	300.0 ± 1.0	14	10.28	−6.882	−0.009
800	35.00	0.149	0.86	7.89	9.5	99.2	34.72	291.1 ± 0.5	10	9.32	−5.932	0.032
850	35.56	0.137	0.17	5.41	13.4	99.7	35.48	297.0 ± 4.2	5	8.90	−5.538	0.061
950	38.73	0.114	0.61	12.10	22.2	99.4	38.52	320.3 ± 0.8	5	8.18	−4.970	0.164
1000	41.28	0.975	0.60	8.62	28.6	99.5	41.08	339.7 ± 0.6	5	7.86	−4.929	0.315
1000	42.36	0.075	0.68	4.21	31.6	99.4	42.13	347.7 ± 0.8	5	7.86	−5.146	0.424
1000	42.50	0.102	0.54	2.81	33.7	99.5	42.32	349.0 ± 1.9	5	7.86	−5.273	0.487
1000	42.49	0.097	1.44	2.14	35.3	98.8	42.04	346.9 ± 1.2	5	7.86	−5.361	0.531
1000	42.80	0.068	0.72	4.53	38.6	99.4	42.56	350.8 ± 0.9	20	7.86	−5.591	0.646
1030	42.44	0.048	0.34	2.17	40.2	99.6	42.31	349.0 ± 0.8	7	7.67	−5.415	0.661
1060	42.64	0.135	1.23	2.82	42.2	99.0	42.25	348.6 ± 1.2	6	7.50	−5.206	0.648
1100	43.13	0.129	0.62	3.67	44.9	99.4	42.92	353.6 ± 0.7	5	7.28	−4.972	0.649
1150	44.15	0.126	1.53	6.98	50.0	98.9	43.67	359.2 ± 0.7	5	7.03	−4.632	0.614
1150	44.15	0.095	0.68	8.96	56.6	99.5	43.92	361.0 ± 1.1	10	7.03	−4.733	0.664
1150	44.16	0.098	1.01	9.92	63.9	99.2	43.84	360.4 ± 0.6	20	7.03	−4.884	0.740
1150	44.14	0.085	0.89	28.30	84.6	99.3	43.85	360.5 ± 0.7	160	7.03	−5.066	0.830
1000	44.76	0.064	1.74	5.02	88.3	98.7	44.22	363.2 ± 0.7	842	7.86	−6.259	0.980
1100	44.73	0.104	0.94	1.52	89.4	99.2	44.43	364.8 ± 1.8	166	7.28	−5.994	1.160
1150	44.12	0.009	0.00	2.02	90.9	99.9	44.11	362.4 ± 1.3	74	7.03	−5.464	1.030
1150	44.23	0.032	0.50	2.71	92.9	99.5	44.05	362.0 ± 1.4	120	7.03	−5.460	1.028
1150	44.40	0.072	1.86	7.08	98.1	98.7	43.82	360.3 ± 0.5	1004	7.03	−5.658	1.126
1150	44.48	0.886	4.43	0.9	98.7	96.7	43.15	355.2 ± 2.5	394	7.03	−5.746	1.170
1150	45.15	0.229	7.70	0.86	99.4	94.7	42.86	353.1 ± 2.0	1002	7.03	−5.937	1.266
1200	41.62	0.674	20.34	0.14	99.5	84.1	35.63	298.2 ± 13.0	22	6.79	−4.884	0.869
1250	43.52	0.114	6.95	0.38	99.7	94.6	41.44	342.5 ± 4.0	20	6.57	−4.210	0.650
1530	45.02	0.275	4.73	0.36	100.0	96.3	43.61	358.7 ± 7.2				

J = 0.005044, weight = 0.08714 g, E = 49.22 kcal/mol, log (D_0/r_0^2) = 4.158 s^{-1}, spherical model.

TABLE 3. MH-10 K-Feldspar Single Crystal

Temperature, °C	$^{40}Ar/^{39}Ar$	$^{37}Ar/^{39}Ar$	$^{36}Ar/^{39}Ar$ (E-3)	$^{39}Ar_K$ (E-14 mol)	Percent $^{39}Ar_K$ Released	$^{40}Ar^*$, %	$^{40}Ar^*/^{39}Ar_K$	Age ± 1 s.d., Ma	Time, min	10000/T, °K	log (D/r^2), s^{-1}	log (r/r_0)
500	126.30	0.2135	48.86	0.70	0.43	83.9	111.90	807.3 ± 9.5	19	12.94	−8.848	0.000
600	40.57	0.0296	12.03	3.03	2.28	87.3	36.98	308.6 ± 3.2	13	11.45	−7.246	0.000
700	36.01	0.0555	18.41	10.80	8.90	83.6	30.54	258.5 ± 2.7	19	10.28	−6.225	0.118
750	34.76	0.0476	3.19	8.69	14.21	95.8	33.78	283.9 ± 2.9	12	9.78	−5.785	0.168
790	35.51	0.0566	2.793	9.22	19.84	96.2	34.65	290.6 ± 2.8	16	9.41	−5.695	0.321
830	37.71	0.0549	1.777	9.13	25.41	97.6	37.15	309.9 ± 3.6	10	9.07	−5.348	0.331
870	39.81	0.0417	2.469	6.42	29.33	96.5	39.05	324.4 ± 3.2	8	8.75	−5.300	0.479
910	42.05	0.0320	1.557	11.90	36.62	97.8	41.55	343.3 ± 3.3	20	8.45	−5.320	0.650
950	44.73	0.0203	2.931	6.93	40.85	96.6	43.83	360.3 ± 3.4	11	8.18	−5.197	0.734
990	44.76	0.0185	2.264	8.58	46.09	97.2	44.06	362.1 ± 3.3	13	7.92	−5.099	0.824
1030	45.26	0.0214	4.024	6.27	49.92	96.0	44.04	361.9 ± 3.8	12	7.67	−5.130	0.974
1070	44.49	0.0321	2.965	8.40	55.05	96.8	43.58	358.5 ± 3.5	12	7.45	−4.934	0.995
1100	45.68	0.0384	5.838	7.82	59.82	94.9	43.92	361.0 ± 3.6	14	7.28	−4.955	1.096
1100	46.75	0.0103	9.419	6.11	63.56	92.2	43.94	361.1 ± 3.5	22	7.28	−5.193	1.216
1160	46.83	0.0460	5.722	4.78	66.47	94.9	45.10	369.8 ± 3.9	8	6.98	−4.806	1.183
1190	46.62	0.0204	3.832	13.70	74.84	96.9	45.46	372.4 ± 4.0	9	6.84	−4.301	1.006
1220	46.53	0.0122	7.607	2.26	88.61	94.6	44.25	363.5 ± 3.5	11	6.70	−3.915	0.888
1250	55.04	0.0400	34.020	10.50	95.05	80.5	44.96	368.7 ± 3.7	35	6.57	−4.396	1.198
1400	49.67	0.0669	12.310	8.11	100.00	58.0	46.00	376.5 ± 3.6				

J = 0.005044, weight = ~0.5 g, E = 49.46 kcal/mol, log (D_0/r_0^2) = 5.1365 s^{-1}, spherical model.

TABLE 4. MH-42 K-Feldspar Single Crystal

Temperature, °C	$^{40}Ar/^{39}Ar$	$^{37}Ar/^{39}Ar$	$^{36}Ar/^{39}Ar$ (E-3)	$^{39}Ar_K$ (E-14 mol)	Percent $^{39}Ar_K$ Released	$^{40}Ar^*$, %	$^{40}Ar^*/^{39}Ar_K$	Age ± 1 s.d., Ma	Time, min	10000/T, °K	log (D/r^2), s^{-1}	log (r/r_0)
500	121.80	0.0574	13.520	1.25	0.58	92.3	117.80	835.2 ± 7.8	12	12.94	−7.435	0.013
600	25.73	0.0013	1.778	6.87	3.77	93.7	25.15	213.6 ± 0.8	22	11.45	−6.083	−0.029
700	31.02	0.0099	15.190	9.21	8.05	84.1	26.50	224.4 ± 2.4	10	10.28	−5.179	0.016
750	30.93	0.0094	2.040	9.66	12.54	96.2	30.29	254.3 ± 2.6	15	9.78	−5.093	0.186
780	30.56	0.0446	1.328	4.67	14.71	95.2	30.13	253.1 ± 2.9	10	9.50	−5.111	0.314
810	31.23	0.0100	0.895	5.31	17.18	95.3	30.93	259.3 ± 2.5	19	9.23	−5.265	0.506
850	32.48	0.0157	3.641	4.35	19.20	92.6	31.37	262.8 ± 3.0	16	8.90	−5.220	0.624
850	33.60	0.0508	5.411	2.25	20.25	87.0	31.97	267.4 ± 3.2	15	8.90	−5.446	0.737
850	34.76	0.1088	11.570	1.88	21.12	81.3	31.31	262.3 ± 3.4	20	8.90	−5.623	0.825
900	33.53	0.0782	6.390	2.50	22.28	89.8	31.61	264.7 ± 3.6	9	8.53	−5.135	0.739
950	34.01	0.0413	4.059	4.66	24.45	93.8	32.78	273.7 ± 2.7	10	8.18	−4.879	0.760
1000	33.83	0.0340	3.511	5.75	27.12	94.6	32.76	273.5 ± 2.8	8	7.86	−4.646	0.780
1050	34.50	0.0094	3.024	11.50	32.49	96.1	33.57	279.8 ± 3.0	12	7.56	−4.457	0.812
1090	34.30	0.0030	3.891	9.35	36.83	95.2	33.11	276.3 ± 2.7	8	7.34	−4.307	0.831
1120	35.75	0.0057	3.815	9.82	41.40	95.5	34.58	287.6 ± 2.8	8	7.18	−4.233	0.862
1150	35.12	0.0160	3.452	11.50	46.76	96.0	34.07	283.7 ± 2.7	8	7.03	−4.111	0.865
1170	35.46	0.0135	3.610	17.30	54.79	96.1	34.36	285.9 ± 2.7	11	6.93	−4.013	0.859
1180	35.38	0.0131	2.592	10.90	59.87	96.6	34.58	287.6 ± 2.7	9	6.88	−4.072	0.909
1200	35.76	0.0095	2.983	13.40	66.12	96.6	34.84	289.6 ± 2.8	8	6.79	−3.845	0.834
1220	38.08	0.0000	5.005	27.00	78.67	95.6	36.57	302.8 ± 3.2	10	6.70	−3.505	0.703
1240	38.40	0.0058	4.525	24.40	90.02	95.6	37.03	306.3 ± 2.9	9	6.61	−3.244	0.610
1280	39.75	0.0062	7.334	15.40	97.16	93.3	37.55	310.3 ± 3.2	7	6.44	−2.916	0.519
1400	51.85	0.0442	30.970	6.10	100.00	46.8	42.67	348.8 ± 4.3				

J = 0.004998, weight = ~0.5 g, E = 38.9 kcal/mol, log (D_0/r_0^2) = 3.6 s^{-1}, planar model.

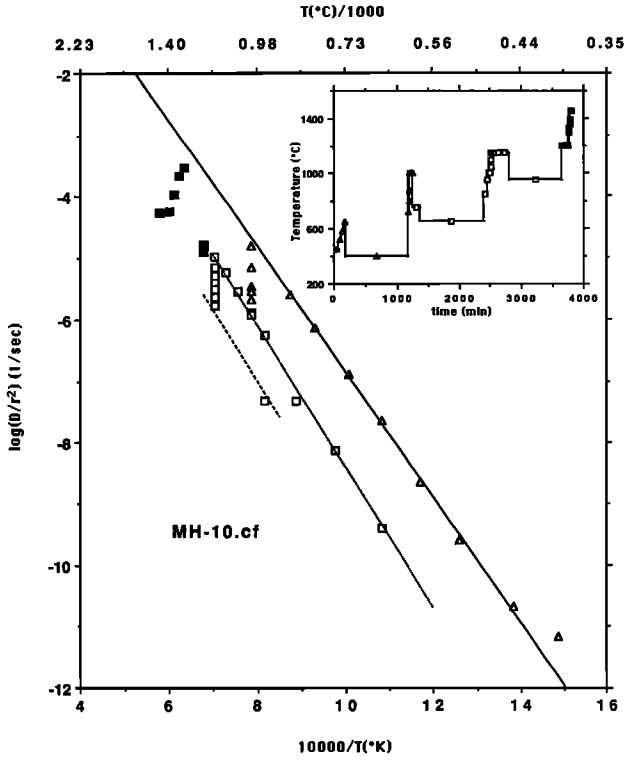

Fig. 2. Arrhenius plot for sample MH-10.cf obtained from a split of MH-10 K-feldspar (separated from the Chain of Ponds pluton) using the extraction temperature schedule shown in the inset. This time, the temperature was raised (open triangles) until it reached 1000°C, then the temperature was kept fixed for several steps to complete the exhaustion of the smallest domains (several open triangles overlap at 1000°C in the inset). The temperature was then reduced for a few steps to assess the activation energy of the next largest domain. This cycle is repeated with isothermal steps at 1150°C (open squares). Finally, the sample was completely degassed at temperatures above the melting point (solid squares). The activation energy of each domain is seen to be very similar.

Lovera et al. [1989] showed this effect by rerunning a split of the sample MH-8 using a cycled schedule. The experiment provided clear evidence that the deviation from linearity in the Arrhenius plot results from a combination of the diffusion domain distribution and the heating schedule use. Prior to approaching the onset of incongruent melting (about 1150°C), the temperature is substantially reduced and later cycled. The advantage of temperature cycling is that by repeatedly reducing the temperature one obtains much more informative data with which to constrain the activation energy of the different size fractions present in the sample.

Figure 2 illustrates how temperature cycling allows a better determination of the activation energies corresponding to the different domains. This Arrhenius plot corresponds to ^{39}Ar data obtained from a split of the MH-10 sample called MH-10.cf. The heating schedule used starts with a monotonically increasing temperatures followed by several steps maintained at a fixed temperature in order to exhaust completely the smallest diffusion domains. After that the temperature was reduced for a few steps to assess the activation energy of the next larger domains, and so on.

Least squares were used to calculate the lines of the two lowest temperatures domains, but the fifth step was not used in the calculation because the large uncertainty introduced by the long step time and the low percent ^{39}Ar released in this step (see the corresponding log (r/r_0) plot in Figure 5). For the largest domain size, only two points were available since at temperatures above about 1150°C (temperature at which the alkali feldspars began to incongruently melt), the diffusion properties of the reactants (leucite plus melt) are considerably different from that of the stable sample (note how the solid squares in Figure 2 do not line up on any earlier trend). This effect was already observed in the monotonic increasing heating experiments. Thus the high-temperature domain line was drawn only to illustrate were a domain with identical E would plot. Extraction temperatures above the onset of melting will result in a loss of important information about the existence and diffusion properties of the largest domains in the sample, which are often found to contain more than 40% of the total argon. The way to avoid this undesirable effect is to extract the ^{39}Ar at temperatures below 1150°C by using larger time steps. Thus another experiment was performed on a second split of MH-10 using thermal cycling (MH-10.bm, Figure 3), but now keeping the temperature below melting until 99% of the argon was released. This time all points of the Arrhenius plot (Figure 3), except the last two black points which represent less than 1% of the total argon released, produced reliable information on the diffusion properties of the sample. Although the activation energy of the largest domain was still not clearly resolved (some scattering appears in the finals steps of Figure 3 due to the low percent ^{39}Ar released) note that the

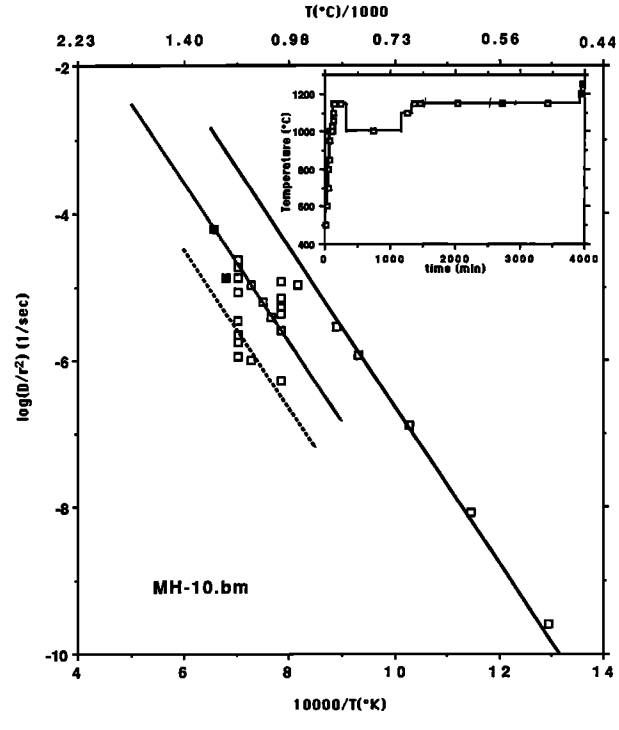

Fig. 3. Arrhenius plot for sample MH-10.bm obtained from another split of MH-10 using the extraction temperatures shown in the inset. The heating schedule was similar to that used in Figure 2, but now the temperature was held below the melting point until 99% of the sample's argon was released. Only two steps (solid squares) were at higher temperatures, releasing less than 1% of the total argon. Again the activation energies of the different domains appear quite similar, keeping in mind that the scatter in the data points for the largest domain are due to very small amounts of gas being released per temperature step.

activation energies of the other two domain sizes appear quite similar (±4 kcal/mol) in both samples and the high-temperature points scatter close to a line drawn parallel to the others two. This time we also used information from other runs of sample MH-10 to calculate the line at lowest temperature by the least squares method. In all the experiments that we have run, which include several reruns of the MH-8, MH-10, and MH-42, the activation energies for the different domain size of each sample agree within about ±4 kcal/mol. A method to resolve differences in activation energies and its implications on the determination of the thermal history are described by *Harrison et al.* [1991].

DETERMINATION OF DOMAINS FROM ^{39}Ar

The distribution of diffusion domains appears to be pivotal to interpreting data from multidomain samples. *Lovera et al.* [1989] calculated the distribution by tedious trial and error. Although cycling produces better resolution of the kinetic parameters than monotonic heating experiments, the size and gas content of each component of the distribution are not clearly displayed. Each datum on an Arrhenius plot has equal weight, although the gas content can be as much as 10 times different. It appears that Arrhenius plots are not an adequate way to plot the ^{39}Ar data for determining the distribution parameters (ρ_j, ϕ_j). *Richter et al.* [1991] proposed an alternate way to view the ^{39}Ar data, which better reveal the properties of the distribution. We present a more detailed discussion of this approach, especially how they can be used to determine the distribution parameters (ρ_j, ϕ_j). Multidomain samples release the first argon like an uniform grain with an effective size r_0 (straight line at low-temperature steps in Figure 1). Thus a function log (r/r_0) can be calculated by subtracting from the low-temperature line determined by the first heating steps, log (D/r_0^2), the real data log (D/r^2), and dividing by two. D is the diffusion coefficient which is assumed to follow the simple Arrhenius equation,

$$D(T) = D_0 e^{-E/RT} \quad (1)$$

where D_0 is the frequency factor, E the activation energy, and R the gas constant. D_0 and E are assumed to be common to all domains in the distribution.

Figure 4 shows the log (r/r_0) plot for both heating schedules applied to the synthetic sample of Figure 1. Note that the difference observed between both Arrhenius plots in Figure 1 does not produce equivalently different log (r/r_0) plots. Only a very small difference due to heating steps of finite duration is observed between the two plots. It appears then that the log (r/r_0) plot is insensitive to the particular heating schedule used for the extraction of argon.

The rapid changes in log (r/r_0) observed at 30% and 80% of cumulative argon released in Figure 4 are associated with the volume fraction of each component, ($\phi_1 \sim 0.3$ and $\phi_1 + \phi_2 \sim 0.8$), while from the relatively horizontal segments one can determine the sizes of the smaller domains, (ρ_1, ρ_2). In Appendix A we present an analytical discussion of these graphs along with the expressions which relate the values of log (r/r_0) obtained from the horizontal segments (we will call them plateaus) with the parameters (ρ_j, ϕ_j).

Log (r/r_0) plots for data from real samples confirm the advantage of plotting the data in this new way. Figure 5 shows the log (r/r_0) from sample MH-10.cf (Arrhenius plot shown in Figure 2) along with its corresponding age spectrum. More than 40% of argon was extracted from this sample at temperatures above 1150°C, which is above the onset of melting. Consequently, there is a change in the diffusion properties of the sample, which in the log (r/r_0) plot produces small apparent domain sizes and results in a loss of important information about the largest domain size. The "small" domains sizes associated with the last ^{39}Ar released in Figure 5 are clearly an artifact, because it makes no sense for these apparently less retentive domains to have been the last to release their argon. Therefore the best heating schedule appears to involve cycling the temperature below the melting point, with repeated isothermal steps, like that applied to the MH-10.bm sample of Figure 3. The corresponding plot of log (r/r_0) versus cumulative percent ^{39}Ar released shown in Figure 6 does not display a lowered value of log (r/r_0) late in release.

A set of distribution parameters (ρ_j, ϕ_j) can be determined from the log (r/r_0) plot using the expression given in Appendix A. A synthetic log (r/r_0) plot calculated using these parameters satisfactorily fits the real data shown in Figure 7, where the actual and synthetic log (r/r_0) plots from sample MH-10.bm are compared.

The K-feldspar PC-88-32 used by *Richter et al.* [1991] also offers a good example of the agreement that one should expect between real and synthetic data. We reproduce in Figure 8 the comparison between both actual and synthetic log (r/r_0) plots obtained from feldspars PC-88-32. The ^{40}Ar/^{39}Ar analytical results and heating schedules of this sample are tabulated by *Richter et al.* [1991].

EFFECT OF DOMAIN PROPERTIES ON THERMAL HISTORY DETERMINATIONS

Determining the components of the domain distribution in a sample from ^{39}Ar data requires an a priori selection of the number of different domain sizes. Even when the number of plateaus observed in the log (r/r_0) plot gives an estimate of the minimum number of domain sizes necessary to produce a satisfactory fitting to the data, a larger number of different domains could produce an equally satisfactory result. Also, the a priori choice of a domain geometry to model the sample affects the resulting volume fractions and sizes of the domains. Equally satisfactory fitting of the real data is obtained using different domain geometries and corresponds with different set of (ρ_j, ϕ_j) parameters and often also different number of domain sizes.

The above discussion points to the fact that the ^{39}Ar data generated by the step heating method are in themselves not enough to determine a unique set of distribution parameters. However, we can investigate the role of these somewhat ad hoc selections (geometry and number of domain sizes) in the final estimate of the thermal history.

A critical question is whether different "acceptable solutions" for the distribution parameters will result in appreciable differences in the estimates of the thermal history? One can assume that two set of parameters (say, (ϕ_j, ρ_j) $j = 1, s$ and (ϕ'_j, ρ'_j) $j = 1, p$) produce a similar calculated release of argon at any step, such that $|^{39}f_m(\phi_j, \rho_j, \zeta_m) - {}^{39}f_m(\phi'_j, \rho'_j, \zeta_m)| < \varepsilon$, where ε is an arbitrary small constant and

$$\zeta_m = \int_0^{t_m} D[T(t')]\, dt'$$

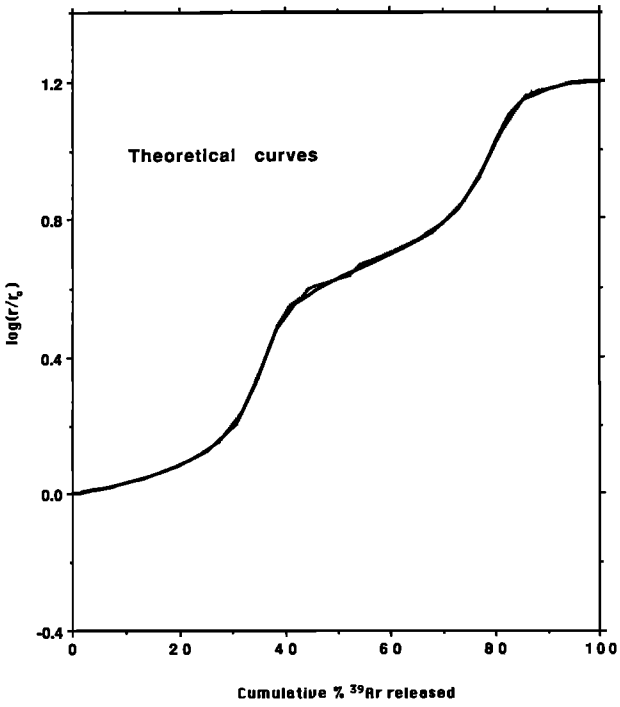

Fig. 4. Theoretical log (r/r_0) plots for the synthetic sample of Figure 1, calculated for both the monotonic (heavy line) and cycled (solid line with symbols) heating schedules shown in the inset of Figure 1. Note that even though the Arrhenius data for the two heating schedules in Figure 1 (heavy line and discrete points) are different, the log (r/r_0) plots show only a very small difference due to the finite temperature steps used to generate the data. Thus the log (r/r_0) plot is seen to be relatively independent of the heating scheduled.

where t_m is laboratory time at the mth step. Note that all "acceptable solutions" will have the same r_0, $\rho_s = \rho_p \equiv 1$, E, and D_0 and thus a common ζ_m. If for any common cooling history all acceptable solutions result in calculated synthetic ages that differ only by order ε, then one would expect that the geometry and number of domain sizes adopted to calculate the set of (ϕ_j, ρ_j) that satisfactorily fits the ^{39}Ar data can be safely used to interpret the ^{40}Ar/^{39}Ar. In other words, different "acceptable solutions" calculated using different geometries and numbers of grains will result in essentially the same estimate of the thermal history.

To calculate the difference between synthetic age spectra obtained from different choices of the amount and geometry of the domain sizes, one must deal with nonlinear equations and integrals making analytical analysis of the general case too cumbersome. However, we present in Appendix B some analytical results for the simple case where the whole thermal history behaves in the manner ($1/T \propto t$) assumed by *Dodson* [1973]; therefore all domains in sample will have the same diffusion time constant τ:

$$\tau = \frac{R}{E(dT^{-1}/dt)} \tag{2}$$

We also illustrate the general case with numerical results, Figure 9 shows three very similar log (r/r_0) plots obtained from distributions with 3, 4, and 5 domains (shown in the inset). All distributions are assumed to have the same Arrhenius parameters, E and D_0. The next step is to calculate age spectra for these distributions using thermal histories that need not be characterized by linear increases of $1/T$ with time. Figure 10 shows the age spectra calculated assuming a constant rate of cooling. Assuming a more complicated thermal history results in the synthetic age spectra shown in Figure 11. This last example was chosen so that the segments of the cooling history affecting different domains of the sample have different cooling rates, in effect very different diffusion time constants, τ_j. Note that in both Figures 10 and 11 there are only small differences in the age spectra obtained using the three different domain distributions. These examples suggest that any set of distribution parameters that allows a satisfactory fit to the Arrhenius and log (r/r_0) plots, will result in an equally satisfactory estimate of the cooling curve based on the ^{40}Ar/^{39}Ar data.

The next question is whether the adoption of a particular geometry might prejudice the interpretation of the ^{39}Ar and ^{40}Ar/^{39}Ar data from multidomain samples? Normalized age spectra calculated for a single grain using planar and spherical geometries show differences in age of about $\pi/2$ in the middle portion of the spectra [see *Lovera et al.*, 1989, Figure 4]. However, in the case of samples with a distribution of diffusion domain sizes this difference becomes less significant. Synthetic normalized age spectra from multidomain samples presented by *Lovera et al.* [1989] show age variations of several τ units in magnitude, which are much larger than the age differences observed in a single-grain age spectrum. In addition, the Arrhenius plots using the same ^{39}Ar data but assuming different domain geometries yield similar activation energies. The difference between their

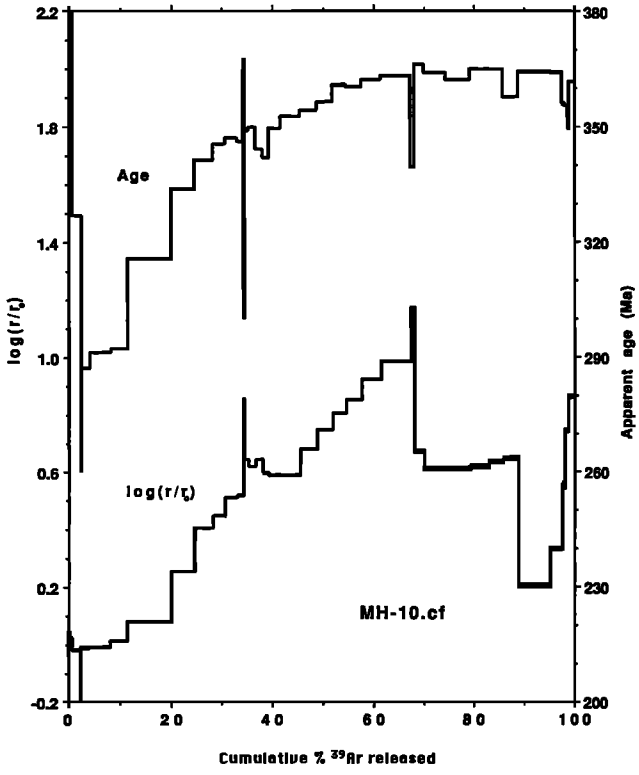

Fig. 5. Log (r/r_0) plot and age spectrum from the remeasured MH-10 sample (MH-10.cf). The last 30% of the argon was released at temperatures above the melting temperature (heavy lines indicates data from above 1150°C), thus the decrease in log (r/r_0) starting at about 70% of the cumulative ^{39}Ar released is not representative of the properties this sample had in its natural setting.

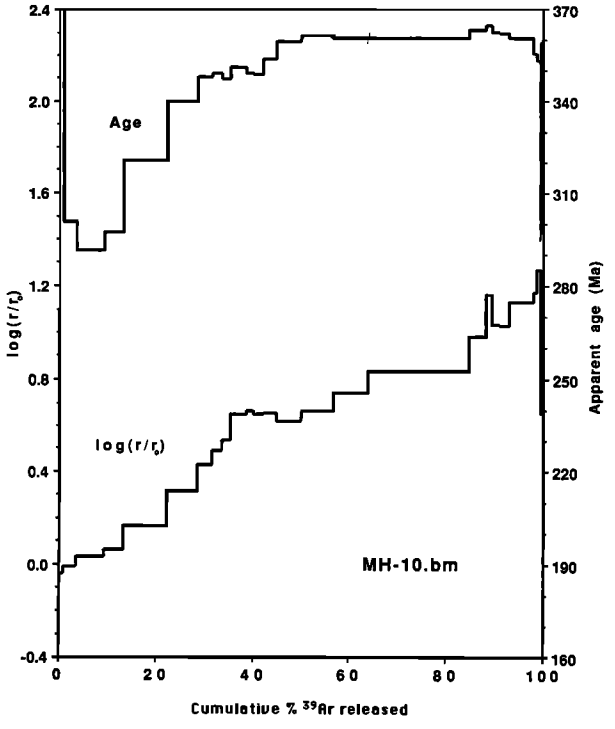

Fig. 6. Log (r/r_0) plot and age spectrum from the remeasured MH-10 sample (MH-10.bm). Since all but the last two extraction temperatures were below the melting point, no anomalously low log (r/r_0) values are observed in the first 99% of the ^{39}Ar released.

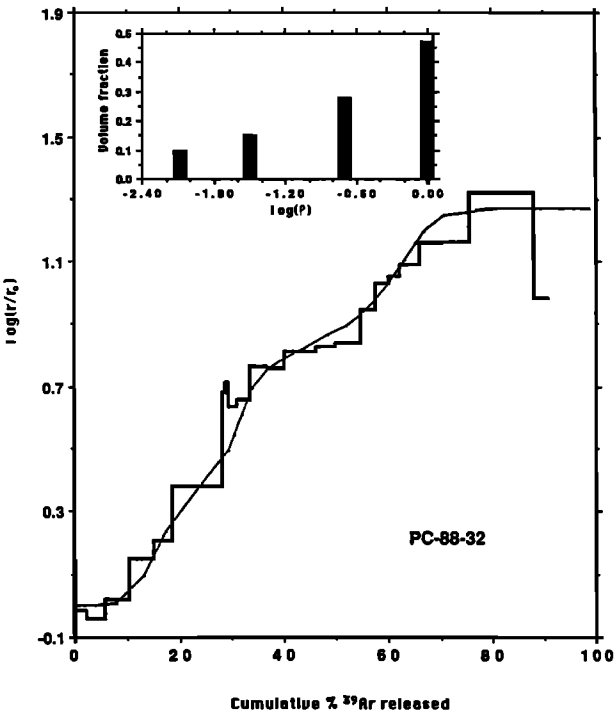

Fig. 8. Log (r/r_0) versus cumulative percent ^{39}Ar calculated for the distribution of domains (largest domain normalized to be one) shown in the inset compared to actual data from Quxu sample PC-88-32 [*Richter et al.*, 1991]. The last two fractions of ^{39}Ar are ignored because they were extracted at such high temperature that the sample experienced incipient melting and therefore the diffusion properties determined from these steps are not representative of the crystalline sample.

Arrhenius plot enters only through the factor log (D_0/r^2), which is also used to calculate the plateau temperatures. Therefore one should obtain essentially the same plateau temperatures assuming any geometry. Finally, the shape of the age spectrum is mainly constrained by the plateau ages of each different diffusion domain size and affected to a lesser extent by the assumed geometry of the domains. Thus one should not expect much difference in the calculated thermal histories obtained by interpreting the data using different geometries. This point is best illustrated using actual data.

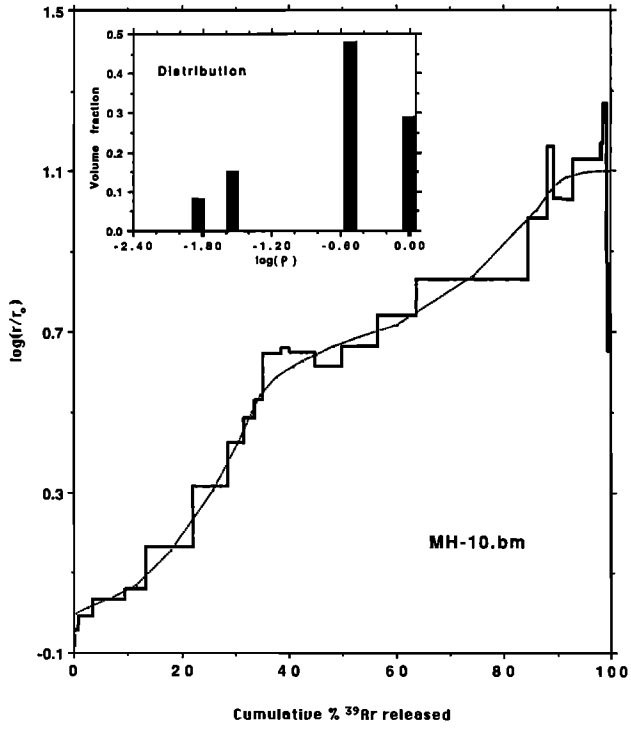

Fig. 7. Log (r/r_0) plot from sample MH-10.bm (solid curve) compared to the theoretical plot (dotted curve) obtained using the distribution parameters shown in the inset.

Figure 12 shows the measured age spectrum and two log (r/r_0) plots of sample MH-10.bm calculated using spherical and planar domains. These plots are compared to the theoretical curves calculated using the distribution of spheres and slabs shown in the inset and the cooling curves shown in the inset to the age spectra plot. Note that even though the spheres and slabs produce different log (r/r_0) plots, requiring different size distributions, the fit to a common age spectrum results in very similar estimates of cooling history. It appears that the specific geometry adopted is not particularly important in determining a thermal history.

All of the samples so far discussed are made up of a mixture of several individual crystals. It is conceivable that the distribution of diffusion domains required to explain the ^{40}Ar/^{39}Ar data is the result of each crystal having a particular domain size. Advances in mass spectrometry now allow for ^{40}Ar/^{39}Ar measurements on small individual crystals, and thus a direct test can be made regarding the existence of multiple domains even in a single crystal.

SINGLE CRYSTALS

Lovera et al. [1989] proposed a distribution of diffusion domain sizes to explain data obtained from alkali feldspar

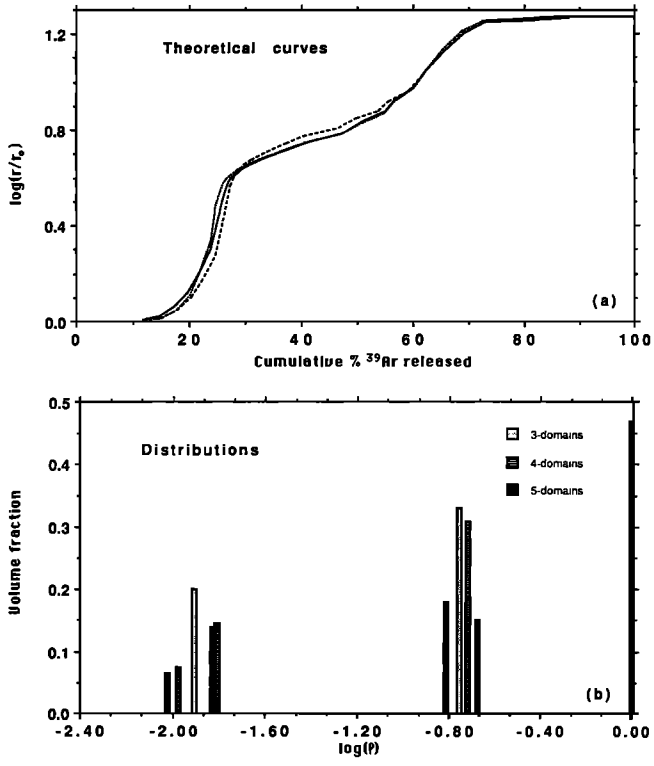

Fig. 9. Log (r/r_0) plots obtained from three synthetic samples having the same diffusion parameters (E, D_0) and distinct but similar distributions. The distributions are shown in Figure 9*b*. Dotted, dashed, and solid lines refer to the samples with 3, 4, and 5 domains, respectively. The largest domain size and its corresponding volume fractions are the same for the three domain distributions (ρ_s = 1, ϕ_s = 0.47).

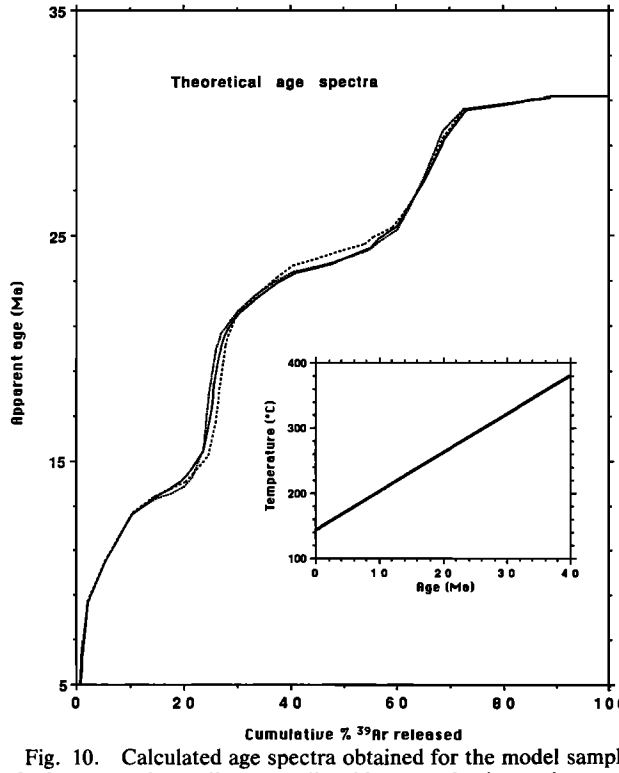

Fig. 10. Calculated age spectra obtained for the model samples of Figure 9 using a linear cooling history. The inset shows the cooling history used. Note that small differences in the log (r/r_0) plot produce equally small differences in the age spectra. Dotted, dashed, and solid lines refer to the samples with 3, 4, and 5 domains, respectively.

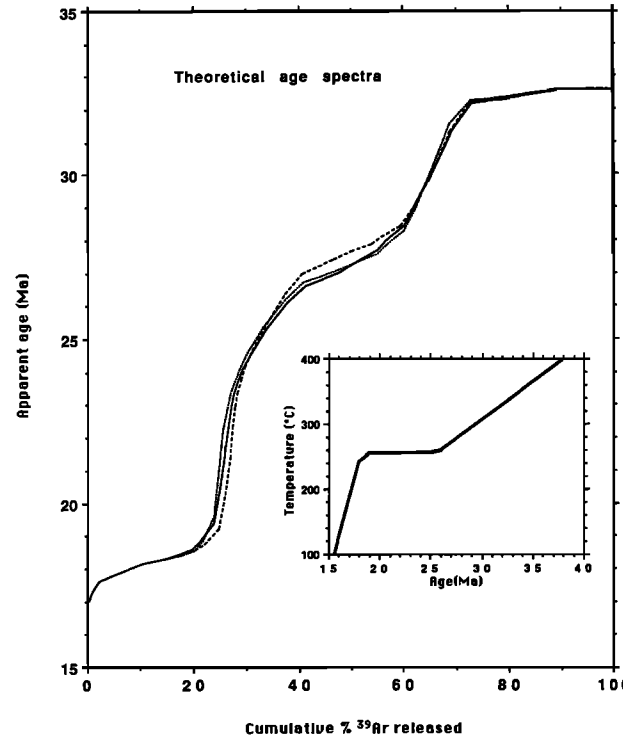

Fig. 11. Same as Figure 10 but using a different cooling history. The cooling history, shown in the inset, is such that the closure temperature of the different domains falls on parts of the thermal history with different rates of cooling. As in earlier examples (Figure 10), only small differences in the age spectra are observed. Dotted, dashed, and solid lines refer to the samples with 3, 4, and 5 domains, respectively.

samples. The new degree of freedom implied by the distribution of sizes allows for much better fits to both the age spectrum and the Arrhenius plot. The fact that the same distribution of sizes improves the fit to these two independent sets of data was taken as evidence that the diffusion domain sizes are actually a physical property of the sample while in its natural environment. Furthermore, we showed that the departure from linear behavior observed in the Arrhenius plot does not depend on temperature but on the cumulative fraction of argon released, which further confirms the existence of distinct diffusion domains. An interesting question is whether a more careful selection of samples in the laboratory could separate diffusion domains of different size, prior to isotopic analysis so that the simpler theory assuming a single uniform diffusion domain size might become applicable. The answer is found in ^{40}Ar/^{39}Ar measurements on single feldspar crystals of the MH-10 and MH-42 samples from the Chain of Ponds pluton. These 500-μm-diameter crystals represent the smallest sample that can be analyzed, because any attempt to crush the sample below this size could lead to a change of the properties of the sample from that while in its natural environment. The data for single crystals are shown in Figure 13, where we plot log (r/r_0) versus cumulative percent ^{39}Ar released from single K-feldspar crystals of MH-10 and MH-42. It is quite clear that even a single crystal contains a distribution of diffusion domains not unlike that found when analyzing an aggregate sample. This suggests that the subdomains arise from the

basic structure of the alkali feldspars and even relatively small single crystals require the multidomain theory.

SUMMARY AND DISCUSSION

The Arrhenius plots for samples with a distribution of diffusion domain sizes depend not only on the activation energy, frequency factor and size distribution, but also on the specific heating schedule (the temperature and duration of each step) used. Thus careful design of heating schedules produces Arrhenius plots that more clearly expose the activation energies of the various size fractions. Data from splits of the MH-10 orthoclase showed that the activation energies of the different domains in the distribution appear similar to within about 4 kcal/mol.

We developed a simple method to determine a set of distribution parameters that produces synthetic Arrhenius plot and log(r/r_0) plot which fit satisfactorily the corresponding actual data. We showed that the determination of the segment of cooling history is not sensitive to changes in the distribution and to the particular choice of the domain geometry provided they fit the same set of ^{39}Ar data. Also, ^{40}Ar/^{39}Ar measurements on single crystals of the MH-10 and MH-42 samples resolve distributions of diffusion domains not unlike those found when analyzing several grains together. Thus the diffusion domains appear to be an intrinsic property of the alkali feldspars, not separable by careful selection of the grains to be analyzed, and the methods developed here are equally necessary when single crystals are use as thermochronometers. The physical nature of these domains is of great interest to us but as yet is imperfectly understood. Our currently efforts are directed at placing constraints on the size and manifestation of these features through microscale imaging (e.g., TEM) and controlled experiments. Results of these experiments underway will hopefully lead us to a refined understanding of the microstructure responsible for the diffusion domains which, in turn, should enhance the clarity of the model.

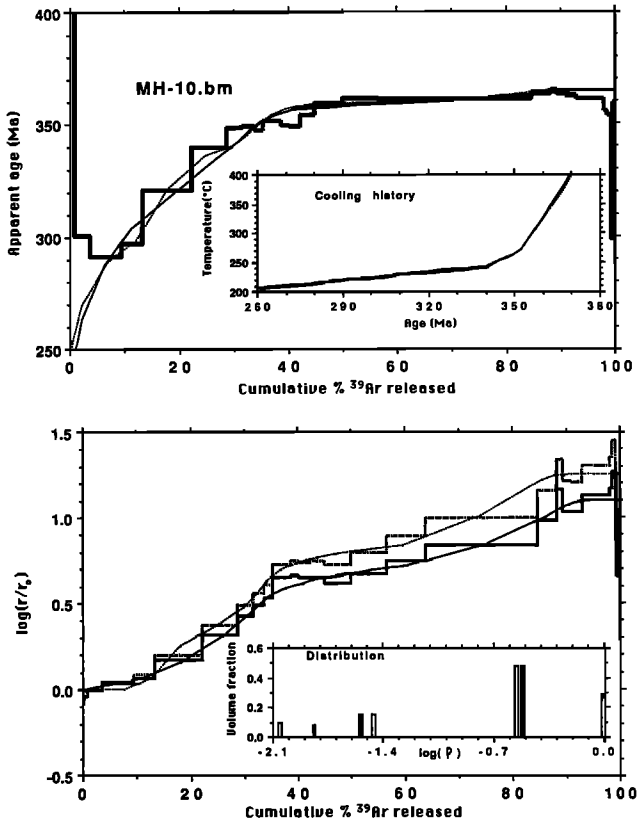

Fig. 12. Interpretations of the data from MH-10.bm using spherical or planar geometry. The actual log (r/r_0) plots and age spectrum are shown in heavy lines. The log (r/r_0) plot for the MH-10.bm data calculated using plane slabs (heavy dotted line), falls above that calculated using spheres (heavy solid line). Both an Arrhenius plot and a log (r/r_0) plot require that the geometry be specified and will differ depending on what geometry is assumed. The distributions obtained by fits to the log (r/r_0)plots are shown in the inset, with open columns for slabs and solid columns for spheres. Theoretical log (r/r_0) plots and age spectra were calculated for these distributions and are shown by dotted and dashed lines for the cases of planar and spherical geometry, respectively. The cooling history determined by fitting the age spectrum assuming each geometry is shown in the inset to the age spectra plot. Note that no appreciable difference in cooling history results from using one or the other geometry.

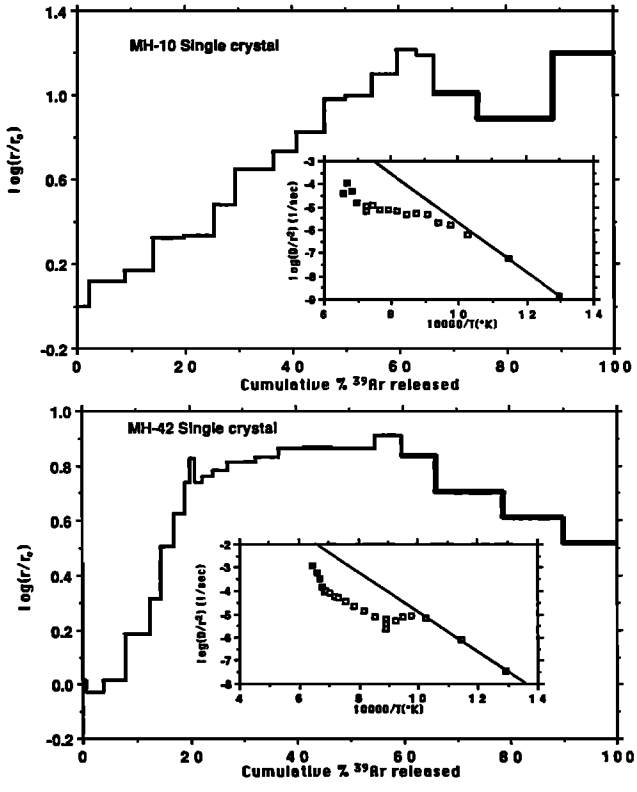

Fig. 13. Log (r/r_0) plots for single crystals separated from the Chain of Ponds pluton samples. The corresponding Arrhenius plots are shown in the insets. The log (r/r_0) plots of the single crystal samples show a distribution of diffusion domains sizes very similar to that of aggregate samples. The solid symbols in the Arrhenius plots and the heavy lines in the log (r/r_0) plots are for data obtained at temperatures above the onset of melting and thus should be ignored.

APPENDIX A: A SIMPLE METHOD TO DETERMINE THE DOMAIN SIZE DISTRIBUTION

The theory for multidomain samples [*Lovera et al.*, 1989] shows that a sample containing several diffusion domain sizes of equal activation energy behaves, for the first release of argon, like a uniform grain with an effective size given by

$$r(\phi_j, \rho_j) = r_0 = \left\{ \sum_{j=1}^{s} \left(\frac{\phi_j}{\rho_j} \right) \right\}^{-1} \quad \text{(A1)}$$

where s is the number of different domain sizes in the sample.

As the extraction of gas continues, the exhaustion of the smallest domain size produces a change in the sample's effective size which will now reflect the characteristic of only the larger domains in the distribution. This property is better displayed if one subtracts from the function log (D/r_0^2) corresponding to a uniform grain with effective size r_0, the multidomain sample data, log (D/r^2). Dividing this difference by two, one gets log (r/r_0), which represents the departure of the apparent grain size r from r_0. A plot of log (r/r_0) versus the cumulative percent ^{39}Ar released reveals the gas content of each separate domain size.

An expression for log (r/r_0) in terms of the fraction of argon released $^{39}f_m$ and ζ_m can be obtained using the equations presented by *Lovera et al.* [1989] (Appendix C, equations (C1) and (C3)).

$$^{39}f_m = \sum_{j=1}^{s} \phi_j \left\{ 1 - b \sum_{n=1}^{\infty} a_n^{-2} \exp\left(-\alpha_n^2 \zeta_m / \rho_j^2\right) \right\} \quad \text{(A2)}$$

The constants b and α_n depend on the particular geometry assumed (spherical ($b = 6$, $\alpha_n = n\pi$), planar ($b = 2$, $\alpha_n = (2n - 1)\pi/2$), and cylindrical ($b = 4$, α_n are the roots of the Bessel function J_0)).

In the case of plane slabs, log (r/r_0) can be written as

$$\log(r/r_0) = \log \left\{ \frac{4r_0^{-2}(\zeta_m - \zeta_{m-1})}{\pi[(^{39}f_m)^2 - (^{39}f_{m-1})^2]} \right\}^{1/2} \qquad ^{39}f_m < 0.60 \quad \text{(A3}a\text{)}$$

$$\log(r/r_0) = \log \left\{ \frac{\alpha_1^2 r_0^{-2}(\zeta_m - \zeta_{m-1})}{\ln[(1 - ^{39}f_{m-1})/(1 - ^{39}f_m)]} \right\}^{1/2} \qquad ^{39}f_m > 0.60 \quad \text{(A3}b\text{)}$$

Slightly more complicated expressions are obtained for spheres and cylinders, but they essentially lead to the same results obtained below for plane slabs. Expression (A3) and those for spheres and cylinders become identical in the limits of small and large $^{39}f_m$. Note that when the cumulative fraction of argon released is small, $^{39}f_m \ll 1$, log (r/r_0) becomes equal to zero by construction. As the extraction of gas continues, the exhaustion of the smallest domain sizes makes the function rise until it reaches the value $-\log(r_0)$, provided the size of the largest grain was normalized to one. Also, the local plateau observed around 50% ^{39}Ar released in Figure 4 reflects the exhaustion of the smallest domain size. Thus, one can approximate $^{39}f_m$ in this part of the spectrum, as

$$^{39}f_m = \phi_1 + 2 \sum_{j=2}^{s} \left(\frac{\phi_j}{\rho_j} \right) \left(\frac{\zeta_m}{\pi} \right)^{1/2} \quad \text{(A4)}$$

Substitution into equation (A3) gives

$$\log(r/r_0) \cong \log \left\{ \frac{r^{*2}(^{39}f_m - \phi_1)}{r_0^2 {}^{39}f_m} \right\}^{1/2} \quad \text{(A5)}$$

where,

$$r^* = \left\{ \sum_{j=2}^{s} \left(\frac{\phi_j}{\rho_j} \right) \right\}^{-1} \quad \text{(A6)}$$

We have assumed that $^{39}f_m < 0.60$, and $\zeta_m - \zeta_{m-1} \ll \zeta_m$, (a similar result is obtained for $^{39}f_m > 0.60$). The approximation obtained in equation (A.5) shows that log (r/r_0) rises from a value of zero for $^{39}f_m < \phi_1$ to a value close to log (r^*/r_0) when $^{39}f_m > \phi_1$. An estimate of how fast this function changes, is given by the derivative of the approximation of log (r/r_0) with respect to $^{39}f_m$ (A.5),

$$\frac{\partial \log(r/r_0)}{\partial {}^{39}f_m} \cong \frac{1}{2(^{39}f_m - \phi_1)} \frac{\phi_1}{{}^{39}f_m} \quad \text{(A7)}$$

Equation (A7) corroborates the result observed in Figure 4, that a sharp change in the log (r/r_0) occurs when $^{39}f_m \sim \phi_1$. A similar expression can be obtained when $^{39}f_m \sim \phi_1 + \phi_2$, such that the intermediate domain size is exhausted. The relative size of the domains can be determined from the plateaus values log (r^*/r_0) and $-\log(r_0)$, while the gas content of each domain can be estimate from the values of cumulative percent ^{39}Ar released where rapid changes in log (r/r_0) take place. A similar result can be obtained for samples containing more than three domain sizes provided that they are well separated in size.

APPENDIX B: EFFECT OF DIFFERENT DOMAIN SIZE DISTRIBUTIONS

When the whole thermal history behaves in the way assumed by *Dodson* [1973] (i.e., $1/T \propto t$), *Lovera et al.*, [1989] found that the normalized age can be written as

$$\Delta \text{ age}_m/\tau = \frac{-2 \sum_{j=1}^{s} \phi_j \rho_j^{-2} \sum_{n=1}^{\infty} \ln(\alpha_n \rho_s / \alpha_1 \rho_j) \exp\left(-\alpha_n^2 \zeta_m / \rho_j^2\right)}{\sum_{j=1}^{s} \phi_j \rho_j^{-2} \sum_{n=1}^{\infty} \exp\left(-\alpha_n^2 \zeta_m / \rho_j^2\right)} \quad \text{(B1)}$$

where Δ age $_m/\tau$ represents the different in ages relative to the age of the last argon released in units of τ.

Now, we will calculate the difference in normalized ages obtained for two similar domain size distributions. In order to simplify the calculation further, we assume that the relation between both distribution is as follows:

$$\phi_1 = \phi_1' + \phi_2' + \varepsilon \qquad \phi_2 = \phi_3' - \varepsilon$$

$$\rho_1 = \rho_1' - \varepsilon = \rho_2' + \varepsilon \qquad \rho_2 = \rho_3' = 1 \quad \text{(B2)}$$

It is also assumed that both distributions have equal diffusion parameters (E, D_0) and satisfy all the constraints imposed by the Arrhenius plot and normalization. Recall that

$$\sum_{j=1}^{s} \phi_j = 1$$

It is easy to verify that $|{}^{39}f_m(\phi_j, \rho_j) - {}^{39}f_m(\phi_j', \rho_j')|$ is order ε, which assures that the distribution produces similar log (r/r_0) plots.

Let $\Delta a = |\text{Age}_m(\phi_j, \rho_j, \zeta_m)/\tau - \text{age}_m(\phi_j', \rho_j', \zeta_m)/\tau|$; the ρ normalization insures that Δa is zero for sufficiently large ζ_m (that is to say, when only the largest domain size contributes to the argon released).

Defining

$$ {}^{40}g(\phi_j, \rho_j, \zeta_m) = 2 \sum_{j=1}^{5} \frac{\phi_j}{\rho_j^2} \sum_{n=1}^{\infty} \ln(\alpha_n/\alpha_1\rho_j) \exp(-\alpha_n^2\zeta_m/\rho_j^2) \tag{B3a} $$

$$ {}^{39}g(\phi_j, \rho_j, \zeta_m) = 2 \sum_{j=1}^{5} \frac{\phi_j}{\rho_j^2} \sum_{n=1}^{\infty} \exp(-\alpha_n^2\zeta_m/\rho_j^2) \tag{B3b} $$

The ^{40}g and ^{39}g are proportional to the ^{40}Ar and ^{39}Ar released at each heating step. From equations (B1) and (B2) one finds

$$ \Delta a = \left| \frac{{}^{40}g'}{{}^{39}g'} - \frac{{}^{40}g}{{}^{39}g} \right| \tag{B4} $$

where, ${}^{40}g' = {}^{40}g(\phi_j', \rho_j', \zeta_m)$ and ${}^{39}g' = {}^{39}g(\phi_j', \rho_j', \zeta_m)$.

Now, a series expansion in ε of $^{40}g'$ and $^{39}g'$ leads to

$$ \Delta a < 2 \left| \frac{{}^{40}g + \varepsilon e^{-\alpha_n^2\zeta_m} + O(\varepsilon^2)}{{}^{39}g + \varepsilon e^{-\alpha_n^2\zeta_m} + O(\varepsilon^2)} - \frac{{}^{40}g}{{}^{39}g} \right| \tag{B5} $$

which by neglecting terms of order ε^2, becomes

$$ \Delta a < \varepsilon[2e^{-\alpha_n^2\zeta_m/{}^{39}g}] \tag{B6} $$

Since the term between brackets is finite, the difference in ages is of order ε. This implies, at least in this simple case, that the interpretation of the ^{40}Ar/^{39}Ar data using any "satisfactory" set of distribution parameters will yield essentially the same estimate of the cooling history.

Acknowledgments. We would like to express our gratitude to Matt Heizler for his technical assistant. We very much appreciate B. Gilletti review which helped improved the final version of this paper. The present study was supported by a Texaco Fellow to O.M.L., a National Science Foundation grant to F.M.R., and a Department of Energy grant to T.M.H.

REFERENCES

Dodson, M. H., Closure temperature in cooling geochronological and petrological systems, *Contrib. Mineral. Petrol.*, *40*, 259–274, 1973.

Gillespie, A. R., J. C. Huneke, and G. J. Wasserburg, An assessment of ^{40}Ar-^{39}Ar dating of incompletely degassed xenoliths, *J. Geophys. Res.*, *87*, 9247–9257, 1982.

Harrison, T. M., and J. D. Fitz Gerald, Exsolution in hornblende and its consequences for ^{40}Ar/^{39}Ar age spectra and closure temperature, *Geochim. Cosmochim. Acta*, *50*, 247–253, 1986.

Harrison, T. M., and I. McDougall, Excess ^{40}Ar in metamorphic rocks from Broken Hill, New South Wales: Implications for ^{40}Ar/^{39}Ar age spectra and the thermal history of the region, *Earth Planet. Sci. Lett.*, *55*, 123–149, 1981.

Harrison, T. M., O. M. Lovera, and M. T. Heizler, ^{40}Ar/^{39}Ar alkali feldspar containing diffusion domains with differing activation energy, *Geochim. Cosmochim. Acta*, in press, 1991.

Heizler, M. T., D. R. Lux, and E. R. Decker, The age and cooling history of the Chain of Ponds and Big Island Pond plutons and the Spider Lake Granite, west-central Maine and Quebec, *Am. J. Sci.*, *288*, 925–952, 1988.

Lovera, O. M., ^{40}Ar/^{39}Ar diffusion from multi-domain samples. *Comput. Geosci.*, in press, 1990.

Lovera, O. M., F. M. Richter, and T. M. Harrison, The ^{40}Ar/^{39}Ar thermochronometry for slowly cooled samples having a distribution of diffusion domain sizes, *J. Geophys. Res.*, *94*, 17,917–17,935, 1989.

McDougall, I., and T. M. Harrison, *Geochronology and Thermochronology by the ^{40}Ar/^{39}Ar Method*, 212 pp., Oxford University Press, New York, 1988.

Richter, F. M., O. M. Lovera, T. M. Harrison, and P. Copeland, Tibetan tectonics from a single feldspar sample: An application of the ^{40}Ar/^{39}Ar method, *Earth Planet. Sci. Lett.*, in press, 1991.

Staudacher, Th., E. K. Jessberger, D. Dorflinger, and J. Kiko, A refined ultrahigh-vacuum furnace for rare gas analysis, *J. Phys. E Sci. Instrum.*, *11*, 781–789, 1978.

Steiger, R. H., and E. Jäger, Subcommission on geochronology: Convention on the use of decay constants in geo- and cosmochronology, *Earth Planet. Sci. Lett.*, *36*, 359–362, 1977.

Turner, G., The distribution of potassium and argon in chondrites, in *Origin and Distribution of the Elements*, edited by L. H. Ahrens, pp. 387–398, Pergamon, New York, 1968.

Zeitler, P. K., Argon diffusion in partially outgassed alkali feldspars: Insights from ^{40}Ar/^{39}Ar analysis, *Chem. Geol.*, *65*, 167–181, 1987.

T. M. Harrison, Department of Earth and Space Sciences, University of California, Los Angeles, CA 90024.

O. M. Lovera, Division of Geological and Planetary Sciences, California Institute of Technology (170-25), Pasadena, CA 91125.

F. M. Richter, Department of the Geophysical Sciences, University of Chicago, Chicago, IL 60637.

(Received May 17, 1990;
revised September 23, 1990;
accepted October 10, 1990.)